

# Spin polarized electrons produced by strong field ionization

Ingo Barth<sup>1</sup> and Olga Smirnova<sup>1</sup>

<sup>1</sup>*Max Born Institute, Max-Born-Str. 2A, 12489, Berlin, Germany*

## Abstract

We show that ionization of noble gas atoms by strong infrared circularly polarized laser field under standard experimental conditions can yield electrons with up to 100% spin polarization in energy resolved measurements. Spin polarization arises due to the interplay of the electron-core entanglement and the sensitivity of ionization in circularly polarized fields to the sense of electron rotation in the initial state.

PACS numbers: 42.50.Hz, 32.80.Rm, 33.80.Wz

Coherent ultrashort light [1] and electron beams [1, 2] produced during the interaction of atoms, molecules and solids with strong infrared laser fields are promising new tools for ultrafast spectroscopy. Photoelectrons extracted by the strong laser field from the tip of a metal wire can form intense, few tens of femtosecond long coherent electron pulses [2], opening new opportunities for ultrafast electron diffraction within a table top setup. Photoelectrons produced via strong field ionization of atoms and molecules can serve as an attosecond probe of optical tunneling [3–6], molecular structure [7, 8] and dynamics [9]; their coherence can be used to record holographic images of atomic core [8, 10]. We show that when produced by ionization in strong infrared circularly polarized field under standard experimental conditions [3–6], coherent ultrashort photoelectron pulses can have high and controllable degree of spin polarization, opening new opportunities for attosecond spectroscopy. One could think that since spin-orbit interaction is a relativistic effect, spin polarization should be negligible in non-relativistic conditions. However, Fano [11] has shown that for one photon ionization it is not the case: weak effects of spin-orbit interaction in the continuum are strongly enhanced in the vicinity of the Cooper minima in photoionization matrix elements, leading to 100% spin polarization for selected energy. In one photon ionization, spin-polarization can also be achieved via ionization from a particular fine structure level of an atom or a molecule [12].

Here we show that high degree of spin polarization arises even if both these mechanisms are not operational. In our mechanism, spin polarization is achieved via spin-orbit interaction in the ionic core and is due to the interplay of (i) the electron-core entanglement and (ii) the sensitivity of ionization in circularly polarized fields to the sense of electron rotation in the initial state.

Consider strong field ionization of noble gas atoms by right circularly polarized field propagating in the positive direction of the  $z$ -axis. For all noble gas atoms except Helium, the outer shell is filled by six  $p$  electrons. Thus, there is no spin-orbit interaction in the ground state and there is equal amount of  $p_+$  and  $p_-$  electrons, 'counter-rotating' and 'co-rotating' with the field. We have recently shown [13, 14] that non-adiabatic tunneling results in high sensitivity of strong field ionization to the sense of electron rotation in the initial state: circularly polarized infrared laser field preferentially removes counter-rotating electrons. Our theoretical prediction has now been confirmed by the experiment [15].

Electron removal leaves the  $p$ -shell open. Spin-orbit interaction splits the states of the ion

with respect to the total angular momentum of the core  $J = 1/2$  and  $J = 3/2$ , providing two ionization channels with slightly different ionization potentials. Electron-core entanglement dictates that in each ionization channel at the moment of ionization the projections of the total angular momentum of the electron  $m_j$  and the core  $M_J$  on the z-axis are exactly opposite.

For the core state  ${}^2P_{1/2}$ , the total core momentum is  $J = 1/2$  and its projection is  $|M_J| = 1/2$ . The orbital momentum of the counter-rotating electron points down, in the negative direction of z-axis. Therefore, the counter-rotating electron correlated to the core state  ${}^2P_{1/2}$  must have spin pointing up to ensure that  $|m_j| = 1/2$ . Thus, 100% selectivity of ionization to the sense of rotation of the electron in the ground state would lead to 100% spin polarization in the channel  $P_{1/2}^2$ . Spin polarization in the channel  ${}^2P_{3/2}$  is less than 100%, since the total momentum of the core  $J = 3/2$  admits both  $|m_j| = 3/2$  and  $|m_j| = 1/2$  of the correlated photoelectron. The ability to separate photoelectron spectra corresponding to  ${}^2P_{3/2}$  and  $P_{1/2}^2$  ionization channels experimentally [16] offers opportunities for controlling spin-polarization of coherent electron beams produced by strong field ionization. Note that similar separation of strong field photoelectron spectra correlated to different core states of a polyatomic molecule has recently been demonstrated in [17] and used to identify different channels in strong field ionization.

To provide quantitative picture of the effect, we extend our method [13, 14] to include spin-orbit interaction. The extension is based on angular momentum algebra and does not contain any further approximations. Pertinent theoretical work in case of linearly polarised fields includes [18, 19].

Nonadiabatic ionization rates for atomic  $p_m$  orbitals ( $m = 0, \pm 1$ ) in left ( $c = -1$ ) or right ( $c = +1$ ) circularly polarized laser fields can be written as a sum over multiphoton channels [13, 14]

$$w_c^{p_m}(\mathcal{E}, \omega, I_p) = \sum_{n \geq n_0}^{\infty} w_{nc}^{p_m}(\mathcal{E}, \omega, I_p), \quad (1)$$

where  $n_0 = (2U_p + I_p)/\omega$ . Summation leads to the following simple expression [13, 14]:

$$w_c^{p_m}(\mathcal{E}, \omega, I_p) = |C_{\kappa l=1}|^2 I_p \frac{\mathcal{E}}{2\mathcal{E}_0} h_c^{p_m}(\gamma) e^{-\frac{2\mathcal{E}_0}{3\mathcal{E}} g(\gamma)}. \quad (2)$$

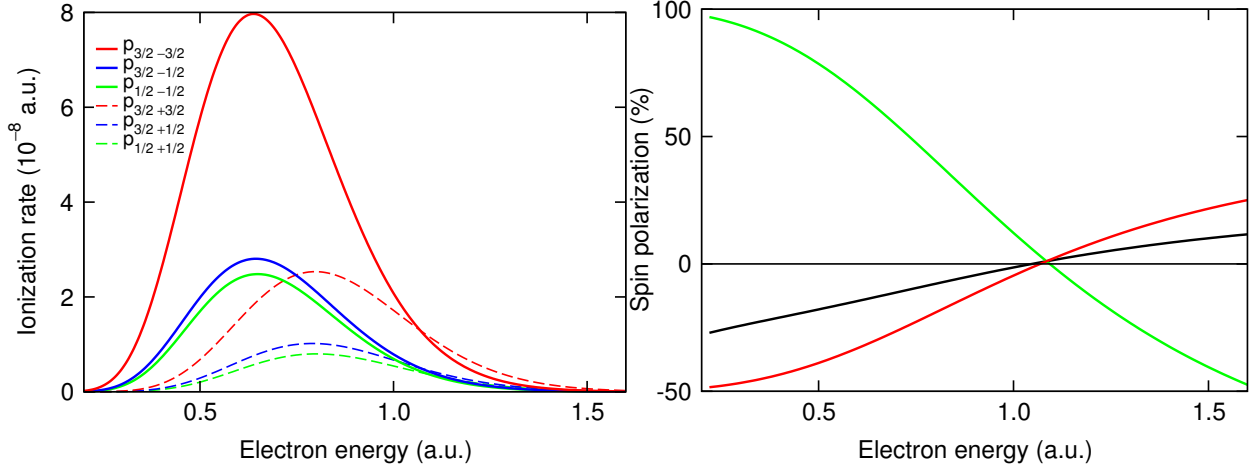


FIG. 1. Left panel shows photoelectron energy distribution (Eq. (11)) for  $p_{jm_j}$  spin-orbitals. Right panel shows spin polarization of photoelectrons (Eq. (14)) resolved on  $^2P_{1/2}$  state of the core (green curve),  $^2P_{3/2}$  state of the core (red curve) and integrated over core states (black curve), for krypton atom, ionization potentials  $I_p^{P_{3/2}} = 0.5145$  a.u. and  $I_p^{P_{1/2}} = 0.5389$  a.u. and right circularly polarized field with frequency  $\omega = 0.057$  a.u. (800 nm) and field strength  $\mathcal{E} = 0.06$  a.u. ( $2.5 \cdot 10^{14}$  W/cm $^2$ )

In Eqs. (1) and (2),  $\mathcal{E}$  is the electric field amplitude,  $\omega$  is the laser frequency,  $I_p$  is the ionization potential,  $U_p = \mathcal{E}^2/(4\omega^2)$  is the pondermotive potential,  $\mathcal{E}_0 = (2I_p)^{3/2}$ ,  $\gamma = \sqrt{2I_p}\omega/\mathcal{E}$  is the Keldysh parameter [20]. The coefficient  $C_{\kappa l=1}$  characterizes the asymptotic behavior of the radial wave function, depending on  $\kappa = \sqrt{2I_p}$  and the orbital quantum number  $l$ , with  $l = 1$  for  $p_m$  orbitals. The exponential factor  $g(\gamma)$  [13, 14] does not depend on the sense of circular polarization  $c = \pm 1$  and on the parameters of atomic orbital. The orbital dependence comes from the prefactors  $h_c^{p_0}(\gamma)$  and  $h_c^{p_{\pm}}(\gamma)$  for  $p_0$  and  $p_{\pm}$  orbitals as shown in Refs. [13, 14] and results in higher ionization rates for  $p_-$  orbitals than for  $p_+$  orbitals in right circularly polarized laser fields ( $c = +1$ ).

The relationship between the ionization rates from the non-relativistic orbitals considered above and the relativistic spin-orbitals  $p_{jm_j}$  with total (orbital and spin) angular quantum number  $j$  and a corresponding magnetic quantum number  $m_j$  obtains using angular momentum algebra. The orbitals  $p_{jm_j}$  can be expanded in the basis of the products of orbitals  $p_m$  and spin functions  $\chi_{sm_s}$  as

$$p_{jm_j} = \sum_{m, m_s} C_{1m, \frac{1}{2}m_s}^{jm_j} p_m \chi_{\frac{1}{2}m_s}, \quad (3)$$

where the expansion coefficients  $C_{lm, sm_s}^{jm_j}$  are the Clebsch-Gordan coefficients with orbital

and spin quantum numbers  $l = 1$  and  $s = 1/2$ , respectively; the corresponding magnetic quantum numbers  $m$  and  $m_s$  are restricted by  $m + m_s = m_j$ . Integrating the corresponding density over the spin variable  $\sigma$  yields the orbital density of spin-orbitals  $p_{jm_j}$

$$\int |p_{jm_j}|^2 d\sigma = \sum_{m, m_s} \left| C_{1m, \frac{1}{2}m_s}^{jm_j} \right|^2 |p_m|^2. \quad (4)$$

The same relations hold for the momentum representation of spin-orbitals  $\tilde{p}_{jm_j}$ , i.e.

$$\int |\tilde{p}_{jm_j}|^2 d\sigma = \sum_{m, m_s} \left| C_{1m, \frac{1}{2}m_s}^{jm_j} \right|^2 |\tilde{p}_m|^2, \quad (5)$$

where  $\tilde{p}_m$  is the momentum representation of orbitals  $p_m$ . Since the ionization rates (Eqs. (1) and (2)) depend linearly on  $|\tilde{p}_m|^2$  (see Refs. [13, 14]), we can express the ionization rate for the spin-orbitals  $p_{jm_j}$  (Eq. (5)) via ionization rates for  $p_m$  orbitals: It yields the general formula for the ionization rates for  $p_{jm_j}$  spin-orbitals

$$w_c^{p_{jm_j}}(\mathcal{E}, \omega, I_p^{P_j}) = \sum_{m, m_s} \left| C_{1m, \frac{1}{2}m_s}^{jm_j} \right|^2 w_c^{p_m}(\mathcal{E}, \omega, I_p^{P_j}), \quad (6)$$

in particular

$$w_c^{p_{\frac{1}{2}\pm\frac{1}{2}}}(\mathcal{E}, \omega, I_p^{P_{\frac{1}{2}}}) = \frac{2}{3} w_c^{p_{\pm}}(\mathcal{E}, \omega, I_p^{P_{\frac{1}{2}}}) + \frac{1}{3} w_c^{p_0}(\mathcal{E}, \omega, I_p^{P_{\frac{1}{2}}}), \quad (7)$$

$$w_c^{p_{\frac{3}{2}\pm\frac{1}{2}}}(\mathcal{E}, \omega, I_p^{P_{\frac{3}{2}}}) = \frac{1}{3} w_c^{p_{\pm}}(\mathcal{E}, \omega, I_p^{P_{\frac{3}{2}}}) + \frac{2}{3} w_c^{p_0}(\mathcal{E}, \omega, I_p^{P_{\frac{3}{2}}}), \quad (8)$$

$$w_c^{p_{\frac{3}{2}\pm\frac{3}{2}}}(\mathcal{E}, \omega, I_p^{P_{\frac{3}{2}}}) = w_c^{p_{\pm}}(\mathcal{E}, \omega, I_p^{P_{\frac{3}{2}}}), \quad (9)$$

or as a sum over multiphoton channels

$$w_c^{p_{jm_j}}(\mathcal{E}, \omega, I_p^{P_j}) = \sum_{n \geq n_0}^{\infty} w_{nc}^{p_{jm_j}}(\mathcal{E}, \omega, I_p^{P_j}), \quad (10)$$

where

$$w_{nc}^{p_{jm_j}}(\mathcal{E}, \omega, I_p^{P_j}) = \sum_{m, m_s} \left| C_{1m, \frac{1}{2}m_s}^{jm_j} \right|^2 w_{nc}^{p_m}(\mathcal{E}, \omega, I_p^{P_j}). \quad (11)$$

Here,  $I_p^{P_j}$  is the  $J$ -dependent ionization potential due to spin-orbit splitting between  ${}^2P_{1/2}$  and  ${}^2P_{3/2}$  states of the ion. The quantum number  $m_s = \pm 1/2$  in equations (6, 11) indicate

projection of the electron spin on the laser propagation direction. Thus, equations (6, 11) provide information on spin-resolved ionization rates. Total spin polarization is proportional to the difference in the total ionization rates for the photoelectrons with spin up  $w_{c\uparrow}(\mathcal{E}, \omega)$  and down  $w_{c\downarrow}(\mathcal{E}, \omega)$  :

$$P_c(\mathcal{E}, \omega) = \frac{w_{c\uparrow}(\mathcal{E}, \omega) - w_{c\downarrow}(\mathcal{E}, \omega)}{w_{c\uparrow}(\mathcal{E}, \omega) + w_{c\downarrow}(\mathcal{E}, \omega)}. \quad (12)$$

Using Eq. (6), total spin-resolved ionization rates can be expressed via  $m$ -resolved ionization rates  $w_c^{pm}$ :

$$w_{c\uparrow,\downarrow}(\mathcal{E}, \omega) = \frac{1}{3} w_c^{p_0}(\mathcal{E}, \omega, I_p^{P_{\frac{1}{2}}}) + \frac{2}{3} w_c^{p_0}(\mathcal{E}, \omega, I_p^{P_{\frac{3}{2}}}) + w_c^{p_{\pm}}(\mathcal{E}, \omega, I_p^{P_{\frac{3}{2}}}) \quad (13)$$

$$+ \frac{2}{3} w_c^{p_{\mp}}(\mathcal{E}, \omega, I_p^{P_{\frac{1}{2}}}) + \frac{1}{3} w_c^{p_{\mp}}(\mathcal{E}, \omega, I_p^{P_{\frac{3}{2}}}),$$

where the upper superscript in  $w_c^{p_{\pm}}$  should be used for spin up ( $\uparrow$ ) and the lower superscript should be used for spin down ( $\downarrow$ ) rates correspondingly.

Prior to the analysis of total spin polarization, it is essential to consider spin polarization resolved on the final electron energy and the final state of the core. Note, that the latter is easily accomplished by energy discrimination of the photoelectron spectra correlated to different core states as in [16, 17]. It is obtained using Eq. (11):

$$P_{nc}(\mathcal{E}, \omega, I_p^{P_J}) = \frac{w_{nc\uparrow}(\mathcal{E}, \omega, I_p^{P_J}) - w_{nc\downarrow}(\mathcal{E}, \omega, I_p^{P_J})}{w_{nc\uparrow}(\mathcal{E}, \omega, I_p^{P_J}) + w_{nc\downarrow}(\mathcal{E}, \omega, I_p^{P_J})}. \quad (14)$$

where the corresponding rates  $w_{nc\uparrow}(\mathcal{E}, \omega, I_p^{P_J})$  and  $w_{nc\downarrow}(\mathcal{E}, \omega, I_p^{P_J})$  are resolved on the number of absorbed photons, i.e. on the final electron energy:  $E_{kin} = (n - n_0)\omega$  [13, 14]. Energy and spin-resolved ionization rates  $w_{nc\uparrow}(\mathcal{E}, \omega)$  are expressed via energy and  $m$ -resolved ionization rates  $w_{nc}^{pm}$  given by Eq. (1) in the same way as in Eq. (13).

Energy and core-state resolved photoelectron spectra for Kr atom are shown in Fig. 1(a) for  $\omega = 0.057$  a.u. and  $\mathcal{E} = 0.06$  a.u. corresponding to 800 nm light with intensity  $2.5 \cdot 10^{14}$  W/cm<sup>2</sup>. Solid and dashed lines represent contributions of counter-rotating and co-rotating electrons, resolved on the core states. The signals coming from co-rotating and counter-rotating electrons are spectrally shifted, reflecting non-adiabatic nature of strong-field ionization [13, 14] for these typical laser parameters. The counter-rotating electrons dominate the low-energy part of the spectrum, whereas the co-rotating electrons dominate

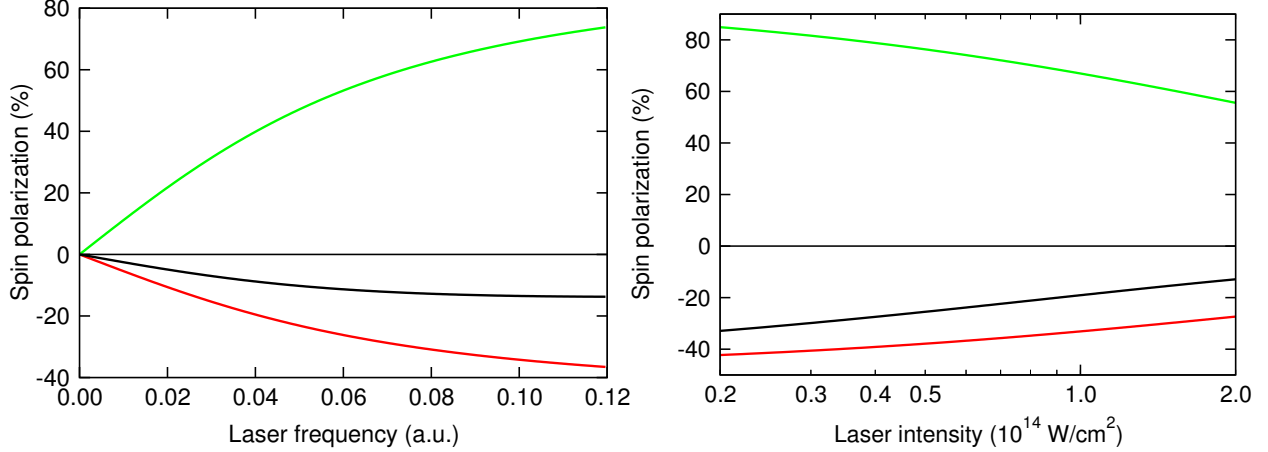


FIG. 2. Control of spin-polarization in strong field ionization of Kr (ionization potentials  $I_p^{P_{3/2}} = 0.5145$  a.u. and  $I_p^{P_{1/2}} = 0.5389$  a.u.) by right circularly polarized laser field. Energy-integrated spin polarization resolved on  $^2P_{1/2}$  state of the core (green curve),  $^2P_{3/2}$  state of the core (red curve) and integrated over core states (black curve). Left panel shows dependence on laser frequency, for the field strength  $\mathcal{E} = 0.06$  a.u. Right panel shows dependence on the laser intensity, for the laser frequency  $\omega = 0.057$  a.u. (800 nm).

the high energy part of the spectrum.

Consider first the electrons correlated to the  $^2P_{1/2}$  state of the core (green curves in Fig. 1(a)). As discussed above, for the  $^2P_{1/2}$  states, the sense of electron rotation uniquely maps into the spin state: the solid green curve corresponds to the spin-up electrons, while the solid dashed curve corresponds to the spin-down electrons. The signal coming from the counter-rotating electron (solid green curve) is much stronger than the signal from the co-rotating electron in the low-energy part of the spectrum, leading to high, close to 100 % spin polarization (see Fig.1 (b), green curve) in the low energy part of the spectrum. Since photoelectron peak correlated to  $^2P_{1/2}$  state is lower in energy than the one for the  $^2P_{3/2}$  state, separating low-energy electrons is efficient method of obtaining 100% spin polarization.

Consider now electrons correlated to the core state  $^2P_{3/2}$ . Had one-to-one mapping between the sense of electron rotation and the orientation of its spin existed for this core state, the respective contribution of the spin-up electron would have been given solely by the red dashed curve, of the spin-down electrons solely by the red solid curve. Thus, the spin polarization would have been given by a curve similar to the green curve in Fig.1 (b), only with the opposite sign.

However, for the core state  $^2P_{3/2}$  the picture becomes more complex, because the total

momentum  $J = 3/2$  has more projections on the z-axis:  $|M_J| = 3/2$  and  $|M_J| = 1/2$ . Each sense of electron rotation in the initial state ( $m$ ) can pair with both projections of the electron spin  $m_s$ . For example, the counter-rotating electron, which dominates the overall signal, can have not only spin down component (red solid curve), but also spin up (blue solid curve) component. Naturally, for the counter-rotating electron the spin down component (solid red curve) dominates the spin up (blue solid curve) component, since  $J = 3/2$  has larger probability to have maximal possible value of the projection  $|M_J| = 3/2$  (i.e. larger Clebsch-Gordan coefficient). For the same reason, the spin-up component of the co-rotating electron (red dashed curve) dominates its spin-down component (blue dashed curve). The interplay of these four spectra is responsible for decreased spin polarization for the electron correlated to the  $^2P_{3/2}$  core state ( compare Fig. 1(b), red curve vs Fig. 1(b), green curve).

Electrons correlated to different core states have spin polarization of opposite sign and therefore the total energy-resolved spin polarization, integrated over the two core states (Fig. 1(b), black curve), is even lower. Such integral energy-resolved spin polarization is particularly relevant when spectral peaks corresponding to different core states can not be resolved, e.g. for short laser pulses.

Spin polarization in strong-field ionization is a manifestation of the non-adiabatic nature of the process. It vanishes in the limit of small Keldysh parameter  $\gamma$  [20], when ionization rates for co-rotating and counter-rotating electrons become equal. Non-adiabaticity increases with increasing  $\gamma$ , offering opportunities for controlling spin polarization of electron beams. Fig. 2 (a,b) shows the degree of spin polarization integrated over the final electron energy and illustrates opportunities for its frequency and intensity control. The degree of spin polarization can be particularly well manipulated via frequency control.

As opposed to state-resolved spin polarization, integrated spin polarization naturally depends on the strength of spin-orbit interaction, i.e. on the energy of spin-orbit splitting  $\Delta E_{SO} = I_p^{P_{1/2}} - I_p^{P_{3/2}}$  in the core. For example, for laser frequency  $\omega = 0.057$  a.u. (800 nm), laser amplitude  $\mathcal{E} = 0.06$  a.u. and right circular polarization, the degree of energy and core state integrated spin polarization is  $-11.0\%$  for krypton,  $-16.4\%$  for xenon, and  $-21.9\%$  for radon, as expected from the respective increase of the spin orbit splitting in the corresponding ions.

Our work opens several new opportunities. First, application of strong laser fields provides the opportunity to increase state-of-the-art density of spin-polarized electron beams



by saturating strong field ionization. Second, it opens new opportunities for strong field and attosecond spectroscopy. In one-photon ionization, spin-polarization spectroscopy offers additional information required for complete characterization of photoionization matrix elements [21], recording the phases between different partial waves. Interesting opportunities for strong-field spin-polarization spectroscopy may arise in molecules, where the co-rotating and counter-rotating initial states are coherent. In this case, spin-polarization will record the relative phase between these states, providing additional information on the process of electron rearrangement during strong field ionization. Finally, relatively strong total spin-polarization signal can be used to probe chiral molecules, extending similar capabilities of the one-photon spin-polarization spectroscopy [21].

We gratefully acknowledge stimulating discussions with M. Ivanov and R. Dörner. This work was supported by the DFG Grant No. Sm 292/2-1.

- 
- [1] F. Krausz, M. Ivanov, *Reviews of Modern Physics* **81** (1), 163, (2009)
  - [2] M. Krger, M. Schenk, M. Frster and P. Hommelhoff, *J. Phys. B* **45**, 074006, (2012)
  - [3] P. Eckle, et al *Nature Phys.* **4**, 565 (2008).
  - [4] P. Eckle, et al *Science* **322** 1525, (2008).
  - [5] H. Akagi, et al *Science* **325**, 1364 (2009)
  - [6] A. P. Pfeiffer, et al *Nature Phys.* **7**, 428 (2011).
  - [7] M. Meckel et al, *Science*, **320**, 1478, (2008)
  - [8] M. Spanner, O. Smirnova, P.B. Corkum, M.Y. Ivanov *J. Phys. B* **37** (12), L243, (2004)
  - [9] C. Blaga et al, *Nature*, **483**, 194, (2012)
  - [10] Y Huismans, et al, *Science* **331** , 61, (2011)
  - [11] U. Fano, *Phys. Rev.* **79**, 131 (1969).
  - [12] N. A. Cherepkov, *J. Phys. B*, **14**, 2165, (1980)
  - [13] I. Barth and O. Smirnova, *Phys. Rev. A* **84**, 063415 (2011); Errata: *Phys. Rev. A* **85**, 029906(E) (2012), *Phys. Rev. A* **85**, 039903(E) (2012).
  - [14] I. Barth and O. Smirnova, *Phys. Rev. A*, submitted (2012), arXiv preprint arXiv:1211.5541, 2012
  - [15] T. Herath, L. Yan, S. K. Lee, and W. Li, *Phys. Rev. Lett.* **109**, 043004 (2012).

- [16] H. Rottke, J. Ludwig, and W. Sandner, J. Phys. B 29, 1479, (1996).
- [17] A. E. Boguslavskiy et al, Science, Vol. 335, 6074 (2012).
- [18] R. Santra, R. W. Dunford, and L. Young, Phys. Rev A 74, 043403, (2006)
- [19] A. S. Kornev and B. A. Zon, Phys. Rev. A **85**, 035402 (2012).
- [20] L. V. Keldysh, Sov. Phys. JETP **20**, 1307 (1965).
- [21] U. Heinzmann and J. H. Dil, J. Phys. 24, 173001, (2012)